Crystal induced phosphorescence from Benz(a)anthracene microcrystals at room temperature

3.1. Introduction:

Room temperature phosphorescence (RTP) has invoked extensive interests among the researchers due to their fundamental importance and potential applications in sensors [121], bioimaging [122], organic lightemitting diodes (OLEDs) [123], optically pumped lasers [124] etc. Many organic luminophores are highly emissive in dilute solution, but their emission decreases with increasing concentration in solution or in aggregated state due to strong intermolecular π–π stacking interaction and collision induced non-radiative decay [125–127]. This phenomenon is known as the aggregation caused quenching (ACQ) effect. On the other hand, many luminescent materials are non-emissive in good solvent but they become emissive in their aggregated form. This phenomenon is called aggregation induced emission (AIE) effect.

This major problem was solved by Tang [128] and Park [129] et al. in 2001 by developing new organic luminescent materials that exhibit stronger emission properties in the solid state than in their solution phase. This property is known as the aggregation induced emission enhancement (AIEE) effect. A variety of luminogens and their derivatives have successfully shown their fluorescence efficiency utilizing this effect, but the most common feature observed in all AIEE active molecules is that they contain a multiaromatic ring with a free rotating component [130, 131]. There are some reports that many luminogenic molecules became more luminescent when their solution was thickened (viscochromism) and cooled (thermochromism) [132], their solids are pressurized (piezochromism) [133] and crystallized (morphochromism) [134] or their aromatic rotors are locked by covalent bonds or hindered by steric effects [135]. The most popular AIE/AIEE mechanismat the single molecular level involves the restriction of intramolecular rotation (RIR), which was primarily proposed by Tang and co-workers [136]. Other mechanisms involve restriction of intramolecular charge transfer (ICT) [137], twisted intramolecular charge transfer (TICT) [138], cis–trans isomerisation [139], and some types of specific molecular packing such as J-aggregation [140,141], dimer/excimer stacking [142], herringbone stacking [143], or even the weakly coupled H-aggregation [144]. Generally, luminogenic materials do not exhibit phosphorescence in the solution state, but they do so at cryogenic temperature or in rigid crystal matrix. The latter phenomenon is known as crystalline induced phosphorescence (CIP) effect [145]. Much effort has been devoted to

synthesize organic nano/μparticles of various sizes and shapes. These include zero dimensional (0-D) spherical or tetrahedral quantum dots [140,146], onedimensional (1-D) nano rods and wires from small organic compounds [147–149], two-dimensional (2-D) nanoplates [150], nanoribbons and nanotubes [151], micro rods, bars, plates [152,153], organic nanoflowers [154], submicrotubes [155] and three dimensional highly symmetrical small organic microcrystals with shapes ranging from cubes through truncated cubes to rhombic dodecahedra [156] etc. Various methods were developed to prepare organic nano/microparticles, such as reprecipitation [157–159], physical vapor deposition [160], solid phase reaction [161], molecular beam deposition [162], laser ablation [163], electrospinning [164], template method [165], and self-organization [166]. Among the above-mentionedmethods, reprecipitation is one of the favored routes towards the cost-effective large-scale production of nano/micro building blocks. Reprecipitation method involves the rapid addition ofmicro amounts of solution of a solute in its good solvent, into macro amounts of a poor solvent. In this process, the sudden change in environment for the organic molecules induces precipitation.

Here, we report a new low dimensional material of Benz(a)anthracene ($\mathbf{P^1}$) microstructures which exhibits crystal induced phosphorescence (CIP) under ultraviolet irradiation. The monomer in solution phase does not show phosphorescence at room temperature unless it is cooled to 77 K [167]. But the novelty of this work is that aggregated $\mathbf{P^1}$ shows phosphorescence at room temperature due to the strong crystal packing. We have also computed second order Fukui parameter for each atomic centre of $\mathbf{P^1}$ as local reactivity descriptor to understand the possible site of interaction between the adjacent $\mathbf{P^1}$ pairs in their aggregated state.

3.2. Experimental Section

3.2.1. Materials

Benz(a)anthracene [$\mathbf{P^1}$]was purchased from Sigma-Aldrich Chemical Corp. Sodium dodecyl sulfate (SDS) was purchased from Merck India Ltd. Tetrahydrofuran (THF) was obtained from S. D. Fine-Chem Ltd. SDS was recrystalized from1:1 ethanol water mixture. THF was distilled from sodium/benzophenone under argon atmosphere to make it free from moisture, oxygen and peroxide. Triply distilled deionized water was used throughout the experiments.

3.2.2. Synthesis of P^I Microparticles

The microstructures of $\mathbf{P^1}$ were synthesized by re-precipitation method using SDS as soft template. In a typical preparation, small volume of 10 mM solution of $\mathbf{P^1}$ in THF was injected

into 5 mL of continuously stirred aqueous SDS at room temperature (25 °C) for 5 min. Clearness of the solution was gradually decreased with increasing concentration of $\mathbf{P^1}$ and a milky white color was appeared. The solution was allowed to stand for overnight. Volume of $\mathbf{P^1}$ and concentration of SDS were varied to synthesize $\mathbf{P^1}$ microstructures. During the synthesis of sample-a, b, c, d, e, f, g, h and i concentration of SDS (3.9 mM) was kept constant and the concentration of $\mathbf{P^1}$ (sample-a: 0.01 mM, sample-b: 0.05 mM, sample-c: 0.09 mM, sample-d: 0.13 mM, sample-e: 0.19 mM, sample-f: 0.38 mM, sample-g: 0.56 mM, sample-h: 0.70mM, sample-i: 0.90mM)was varied in order to examine the effect of $\mathbf{P^1}$ concentration on aggregated structures. On the other hand, sample-j was prepared by injecting 0.5 mL of 10 mM $\mathbf{P^1}$ in THF into 5 mL 20 mM SDS with constant stirring.

3.2.3. Characterization

UV–Vis spectroscopic measurements were carried out in a 1 cm quartz cuvette with a Shimadzu UV-1800 spectrophotometer. Fluorescence spectra were recorded using Hitachi F-7000 fluorescence spectrophotometer. The morphologies of the synthesized nano/microstructures were studied using a ZEISS EVO 18 scanning electron microscope (SEM) with an accelerating voltage of 5 kV. Samples for the SEM study were prepared by placing a drop of the aqueous suspension of particles on a small glass slide followed by solvent evaporation under vacuum. To minimize sample charging, the dried samples were coated with thin gold layer right before SEM study. Time-resolved fluorescence measurements were carried out under ambient conditions using a time correlated single-photon counting (TCSPC) spectrometer [a picoseconds diode laser (IBH, UK)] with the detection wavelength at 410nmfor both the mother solution ($\mathbf{P^1}$ in THF) and sample-c. Excitation wavelength was 336 nm for all the samples. Lamp profiles were measured with a band-pass of 3 nm using Ludox as the scatterer. The decay parameters were recovered using non-linear iterative fitting procedure based on the Marquardt algorithm [168]. The quality of fit was assessed over the entire decay, including the rising edge, and tested with plot of weighted residuals and other statistical parameters e.g. the reduced $\chi 2$ ratio [169]. The signal was detected at magic angle (54.7°) polarization using a Hamamatsu MCP PMT (3809 U). Time resolution of the experimental setup was ~90 ps. Optical microscopy images were taken using an NIKON ECLIPSE LV100POL upright microscope equipped with CCD camera (model no. Nikon DS-Fi l), polarizer-analyzer assembly and 12 V- 100W mercury lamp as excitation source

for emission study. The samples for optical microscopic study were prepared by placing a drop of colloidal solution onto a clean glass slide.

3.2.4. Computational study

In the aggregated structures of molecules, where weak interaction between different atomic centre of similar kind of molecules take place, a second-order local reactivity descriptor (LRD) called second order Fukui function [170–172] may be used instead of electronic density. Density Functional Theory (DFT) based hybrid functional (B3LYP) and 6-31G(d, p) basis set were used to compute the second order Fukui function, $f^{(2)}(r)$ as local reactivity descriptor. Fukui function is defined as the first derivative of $\rho(r)$, electronic charge density with respect to total number of electron (N), at constant external potential, $\upsilon(r)$.

$$f(r)=\left[\frac{\partial\rho(r)}{\partial N}\right]_{\upsilon(r)} \qquad \text{..... (1)}$$

The function $f(r)$ reflects the ability of a molecular site to accept or donate electrons. Higher values of $f(r)$ are related to a high reactivity at point r [170]. Since the number of electrons N is a discrete variable, right and left derivatives of $\rho(r)$ with respect to 'N' have emerged [173]. By applying a finite difference approximation to eq (1), two definitions of Fukui functions depending on total electronic densities are obtained as the followings.

$$f^{+}(r)=\left[\frac{\partial\rho(r)}{\partial N}\right]^{+}_{\upsilon(r)}=\rho_{N+1}(r)-\rho_{N}(r) \qquad \text{..... (2)}$$

$$f^{-}(r)=\left[\frac{\partial\rho(r)}{\partial N}\right]^{-}_{\upsilon(r)}=\rho_{N}(r)-\rho_{N-1}(r) \qquad \text{..... (3)}$$

Where $\rho_{N+1}(r)$, $\rho_{N}(r)$, and $\rho_{N-1}(r)$ are the electronic densities at point 'r' for the system with 'N+1', 'N', and 'N−1' electrons, respectively. The first one, $f^{+}(r)$, is associated to reactivity for a nucleophilic attack so that it measures the intramolecular reactivity at site 'r' toward a nucleophilic reagent. The second one, $f^{-}(r)$, has been associated to reactivity for electrophilic attack so that this function measures the intramolecular reactivity at site 'r' toward an electrophilic reagent [171].

Morell et al. [174-178] have proposed a local reactivity descriptor (LRD) which is called the dual descriptor (DD) $f^{(2)}(r) \equiv \Delta f(r)$. Morell and co-workers used the notation $\Delta f(r)$, but currently it has been replaced by the modern notation $f^{(2)}(r)$ in order to highlight the fact that this is a Fukui function of second order. Its physical meaning is to reveal nucleophilic and electrophilic sites on a molecular system at the same time. Mathematically, it is defined in terms of the derivative of the Fukui function, $f(r)$ [173], with respect to the number of electrons, 'N'. Through a Maxwell relation, this LRD may be interpreted as the variation of 'η' (the molecular hardness) which measures the resistance to charge transfer [179] with respect to υ(r), the external potential. The definition of $f^{(2)}(r)$ is shown as given by Morell et al. [174,175].

$$f^{(2)}(r) = \left[\frac{\partial f(r)}{\partial N}\right]_{\upsilon(r)} \quad \text{..... (56)}$$

As mentioned above, DD allows one to obtain simultaneously the preferable sites for nucleophilic attacks ($f^{(2)}(r) > 0$) and the preferable sites for electrophilic attacks ($f^{(2)}(r) < 0$) into the system at point 'r'. All the computations on **P^1** in this present study were carried out using Gaussian-09 package programs [180].

3.3. Results and Discussion

3.3.1. SEM study

No clear morphology of the particles was observed when the synthesis was carried out in the absence of SDS. While synthesizing the Benz(a)anthracene (**P^1**) microstructures in presence of SDS, we did two set of synthesis where the concentration of SDS and **P^1** were varied for a fixed concentration of **P^1** and SDS respectively. Our SEM (***Fig. 3.1***) study reveals that in both the sets the morphology of particles is rectangular plate shaped and the size of the particle increases with the increasing concentration of **P^1**.

3.3.2. Optical microscopic study

Rectangular plate shaped morphology is clearly obtained for the sample-e, f, g, h, i and j using optical microscopy (***Fig. 3.2***). At low **P^1** concentration, particle sizes are too small to be detected by the present resolution of our optical microscope. Upon UV excitation, micro crystals having clear edges with greenish luminescence are observed. The morphology of **P^1**

microstructure in all the samples are rectangular plate shaped and there is a clear indication that dimension of the particles in two directions (length and breadth) increases with the increasing concentration of **P[1].**

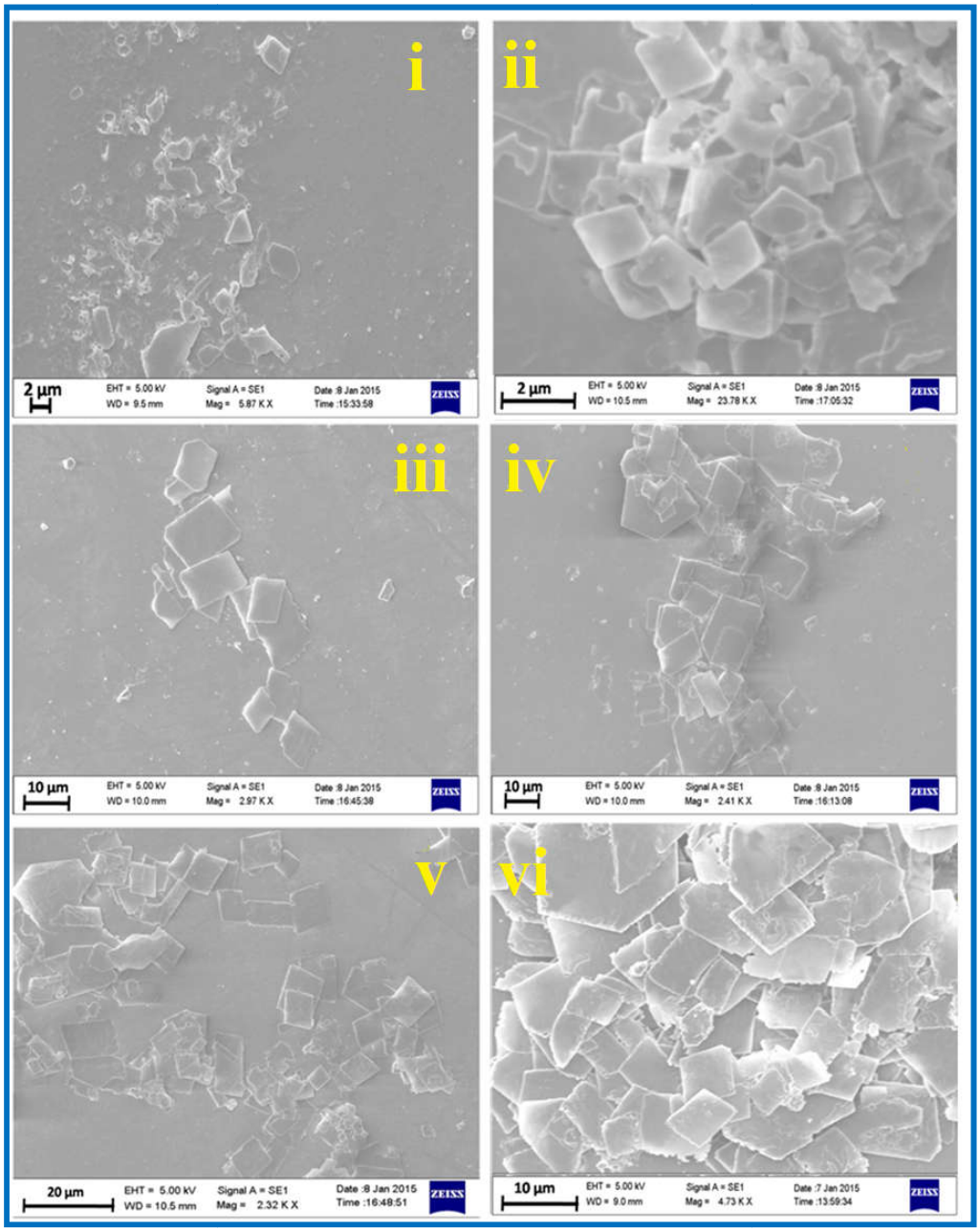

Fig. 3.1: SEM images of **P[1]** microstructures, (i) sample-e, (ii) sample-f, (iii) sample-g, (iv) sample-h, (v) sample-i, (vi) sample-j.

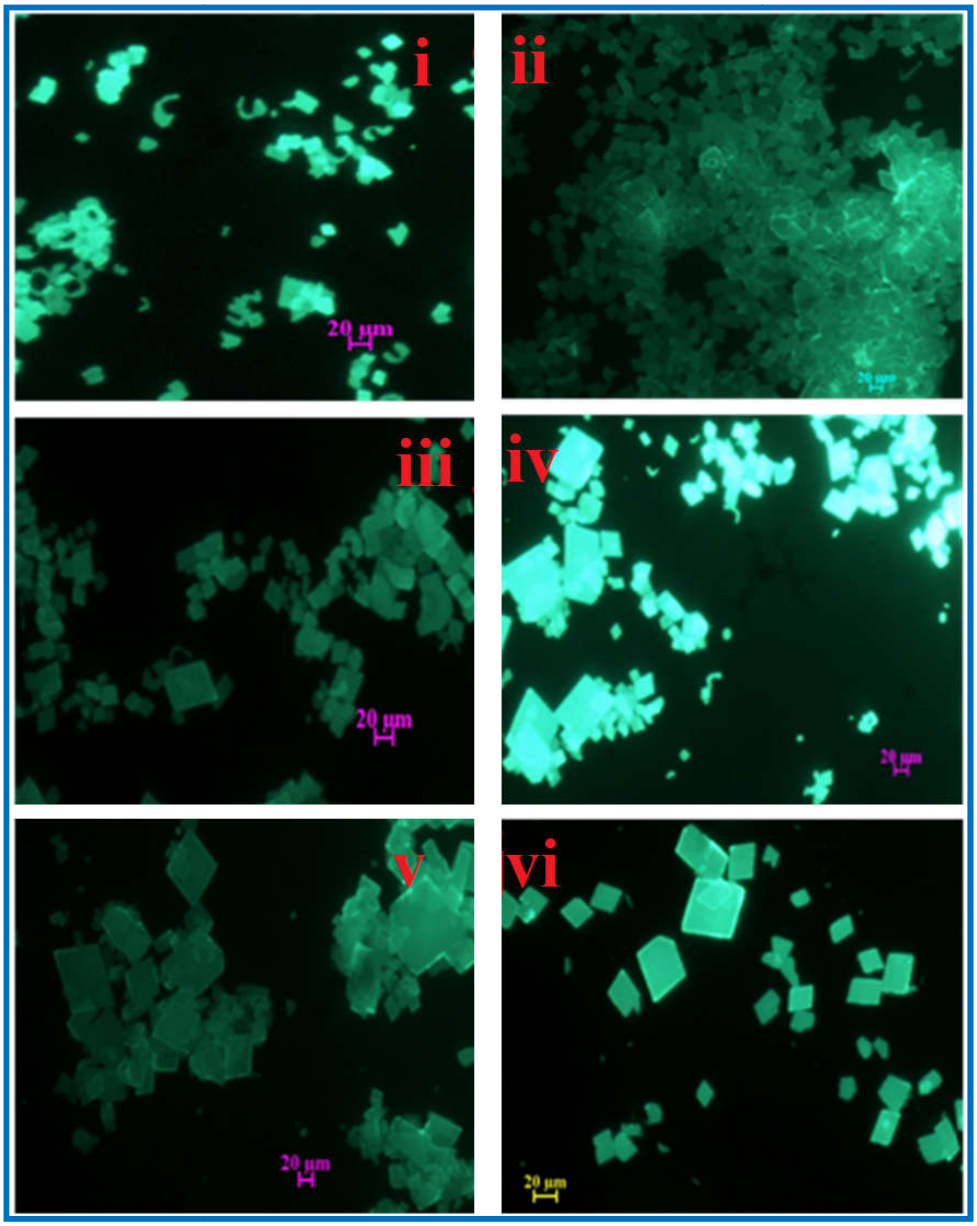

Fig. 3.2: Optical fluorescence microscopy images under UV excitation of (i) sample-e, (ii) sample-f, (iii) sample-g, (iv) sample-h, (v) sample-i, (vi) sample-j.

3.3.3. UV-Vis Study

The UV absorption spectrum of **P**[1] can be divided into two well distinct regions i.e. 300–360 nm and 232–289 nm, corresponding to two types of electronic transitions (***Fig. 3.3***). In case of polyaromatic hydrocarbon like anthracene, pyrene etc., the group of bands with higher energy are associated primarily with excitation direction along the long (a, a′) axis and the group of band

with lower energy are associated with excitation direction along the short (b, b′) axis (Scheme 1) [181].

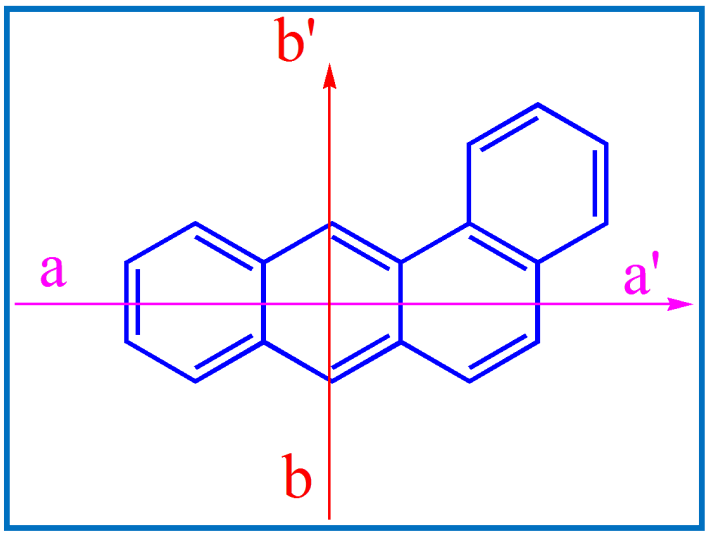

Scheme 3.1: $\mathbf{P^1}$ with its long (a, a') axis and short (b, b′) axis.

The absorption spectra of $\mathbf{P^1}$ hydrosols are red shifted by nearly 36 nm and broadened compared to its monomer absorption. The shift and broadening are likely originated due to strong π–π interaction with the neighboring $\mathbf{P^1}$ molecules in its aggregated structure. In addition, the overall shift of the spectral baseline of samples d-h relative to that of the monomer is attributed to the scattering of light by the larger aggregated structures in solution (***Fig. 3.3***).

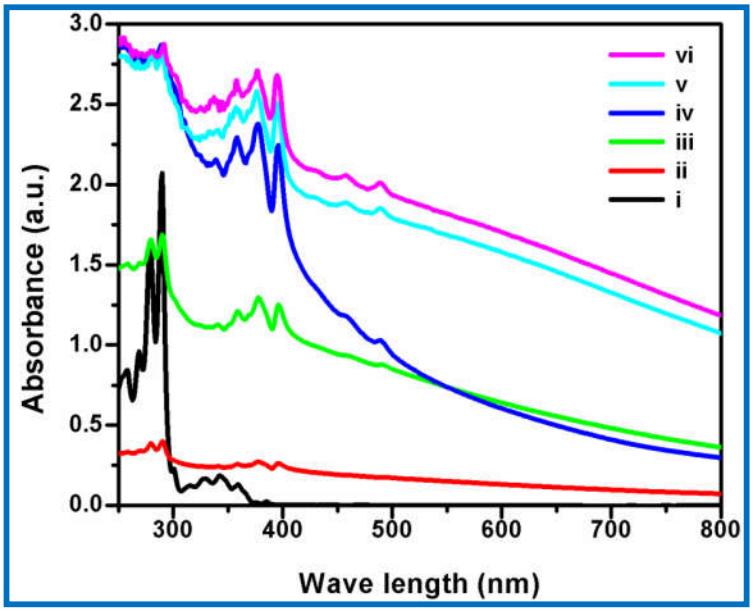

Fig. 3.3: UV–visible absorption spectra of (i) $\mathbf{P^1}$ in THF (ii) sample-d, (iii) sample-e, (iv) sample-f, (v) sample-g, (vi) sample-h.

3.3.4. Emission Study

Photoluminescence (PL) spectra of $\mathbf{P^1}$ in THF and the aggregated hydrosol of $\mathbf{P^1}$are shown in ***Fig. 3.4***. It is observed that the dilute solution (0.6 μM) of $\mathbf{P^1}$ in THF exhibits structured emission band with peak at 387, 410, 434 nm upon 336 nm photo excitation. But the aggregated hydrosol of $\mathbf{P^1}$ exhibits two separate groups of structured emission bands, one at the same position that of $\mathbf{P^1}$ in THF and the other one largely red shifted with vibronic peaks appearing at 493, 528 and 566 nm. It seems that the red shifted structured band arises from some low lying emissive state. It is also observed that PL intensity in the region 350–450 nm decreases relative to that of the mother solution (sample-m: $\mathbf{P^1}$ in THF) with the increasing concentration of $\mathbf{P^1}$ in the hydrosol. This is attributed to aggregation caused quenching (ACQ) effect (***Fig. 3.4***). But PL intensity in the region 490–600 nm of hydrosol increases gradually with increasing concentration of $\mathbf{P^1}$ and we presume that this structured emission arises from some low lying emissive state of rigid crystalline structure of $\mathbf{P^1}$. In order to substantiate this emissive state of $\mathbf{P^1}$, we have carried out time resolved emission study of both the emission region of the aggregates hydrosol and also of the mother solution.

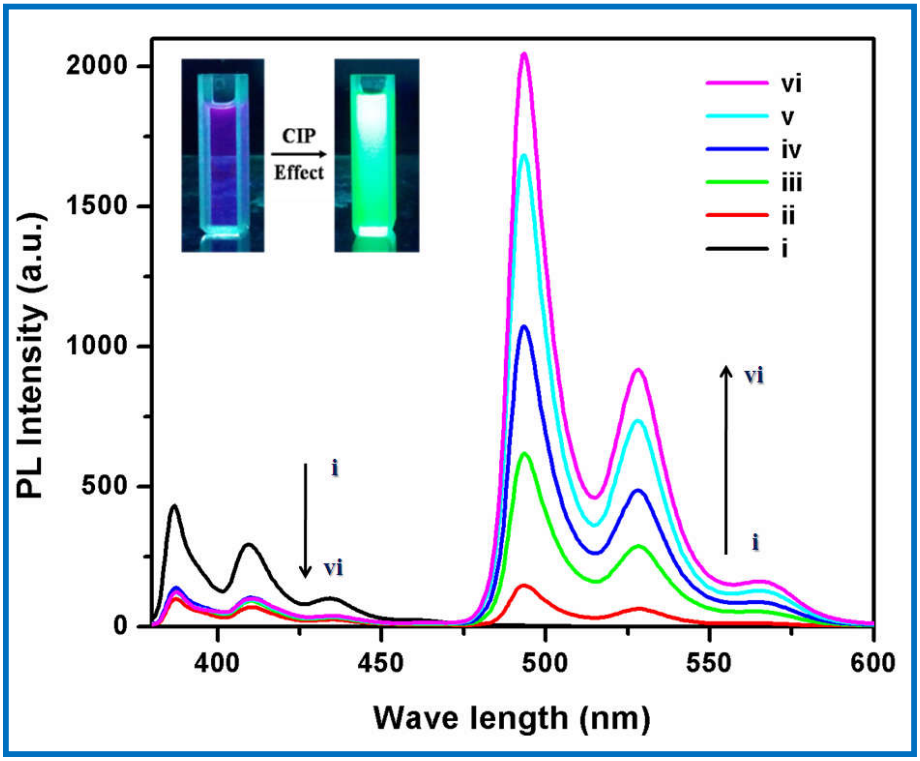

Fig. 3.4: Fluorescence emission spectra of (i) $\mathbf{P^1}$ in THF, (ii) sample-a, (iii) sample-b, (iv) sample-c, (v) sample-d, (vi) sample-e. All emission spectra were taken with 336 nm excitation.

3.3.5. Time resolved emission study

We have carried out time resolved fluorescence study of **P[1]** in THF and aggregated **P[1]** hydrosol with excitation at 336 nm and emission are measured at 410 nm and 493 nm. The decay profile of the monomer and the hydrosol are shown in ***Fig. 3.5***. During the present study, we have prepared a number of set of aggregated hydrosol with increasing concentration of **P[1]** and labeled the hydrosol as sample-a, b, c, d, e, f, g, h, i. We could not measure the fluorescence emission of sample-f to i because of larger size of **P[1]** crystals which are precipitated out from the solution. On the other hand among the sample-a to e, sample-c shows moderately intense fluorescence emission. Since the steady state fluorescence spectral characteristics of sample -a to e are similar, we have used only sample-c showing moderately intense emission intensity for time resolved emission study. The fluorescence decay curve of **P[1]** in THF is fitted with biexponential decay and the observed decay times are 0.86 ns and 13.6 ns respectively (***Table 3.1***). The major component (78%) having lifetime 0.86 ns is the fluorescence lifetime of excited singlet (S_1) state of **P[1]**. There is some early report in the literature that **P[1]** show P-type delayed emission due to its small singlet-triplet energy gap. We presume that the other component (22%) having relatively larger value of lifetime, i.e. 13.6 ns is due to P-type delayed emission from the S_1 state of **P[1]** [182]. On the other hand, fluorescence decay curve of **P[1]** hydrosol monitored at 410 nm shows two components. The major components (92%) have lifetime 0.16 ns and the minor (8%) component have lifetime 22.4 ns. Since in its aggregated structures **P[1]** molecules are close to each other, the 0.16 ns components arises due to self quenching of **P[1]** in its aggregates and the 22.4 ns component is due to P-type delayed emission component from **P[1]** in its aggregated structures. We have also tried to measure the emission lifetime at 493 nm of the aggregated hydrosol, but it shows very long decay component which is beyond the scope of our TCSPC setup. Thus we thought this long live component is due to some low lying long live state i.e. triplet state of **P[1]**. Keeping this in mind, we have used a rotating chopper to cut out the short emission component. The observed emission spectra using chopper is shown in ***Fig. 3.6a***. This spectrum is identical with the phosphorescence emission spectra of **P[1]** as reported by A. Segura Carretero et al. [183]. Thus it is concluded that the red shifted, structured PL emission band (480–600 nm) appearing in the hydrosol corresponds to the phosphorescence emission from the low lying excited triplet state of **P[1]** in its aggregated state. We measured phosphorescence lifetime of the hydrosol by monitoring the emission at 493 nm.

Table 3.1: Fluorescence lifetime of $\mathbf{P^1}$ in THF and its aggregated hydrosols (sample-c) of $\mathbf{P^1}$. (excitation:336 nm).

Sample	Emission wavelength	Contribution (%)	τ_1 (ns)	Contribution (%)	τ_2 (ns)	χ^2
P^1 in THF	410 nm	78	0.86	22	13.6	0.93
P^1 Hydrosol (Sample-c)	410 nm	92	0.16	8	22.4	0.94

Phosphorescence decay curve as shown in ***Fig. 3.6b***, is fitted with bi-exponential decay with a major component (83%) having lifetime 0.12 ms and the minor one (17%) having lifetime 2.32 ms. This 0.12 ms component arises from some low lying triplet state of $\mathbf{P^1}$ in its aggregated form and the long lived (2.32ms) minor component arises from other trap triplet state present within the microcrystals due to micro heterogeneous nature of the aggregated hydrosols. Generally the triplet quantum yield of any organic molecule is very low at normal temperature and low temperature (77 K) is required to observe emission from triplet i.e. phosphorescence emission. But in the present case, the free rotation of the molecule and the large amplitude vibrational modes which are responsible of the transfer the excited energy to other molecules of the same type or to solvent molecules are less probably due to π–π stacking interactions within the aggregated structures. This phenomenon, known as the restricted intramolecular motion (RIM), permits to attain a reasonable excited triplet population, which allows the observation of phosphorescence emission even at room temperature.

3.3.6. Computation of Fukui Parameters as local reactivity descriptor

Our extensive survey of literature shows that there is a report as early as 1938 by Iball et al. [184] on the crystal structure of $\mathbf{P^1}$, but we find difficult to get the possible arrangement of $\mathbf{P^1}$ molecules from these reported single crystal data. Also, Friedlander et al. [185] successfully

grew the single crystal and they also reported an incomplete refinement of **P**[1] crystal structure data.

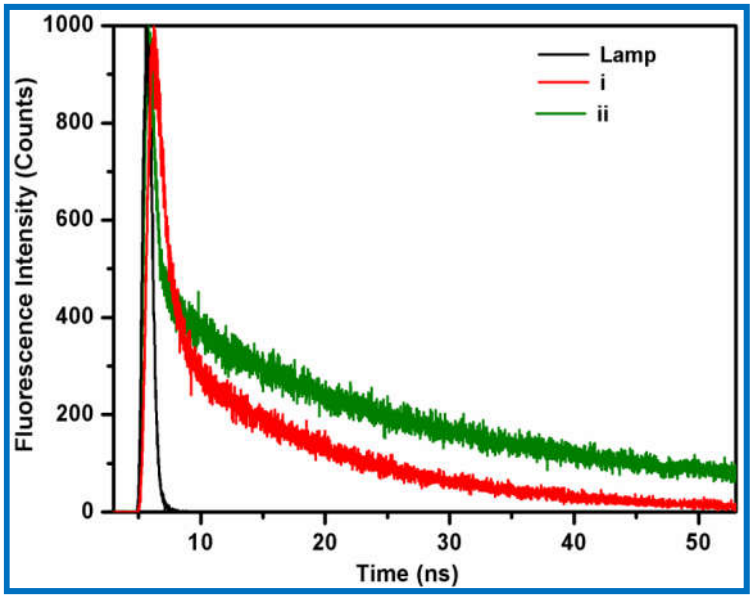

Fig. 3.5: The fluorescence decay profiles of (i) **P**[1] in THF, (ii) sample-c; excitation wavelength: 336 nm, emission wavelength: 410 nm

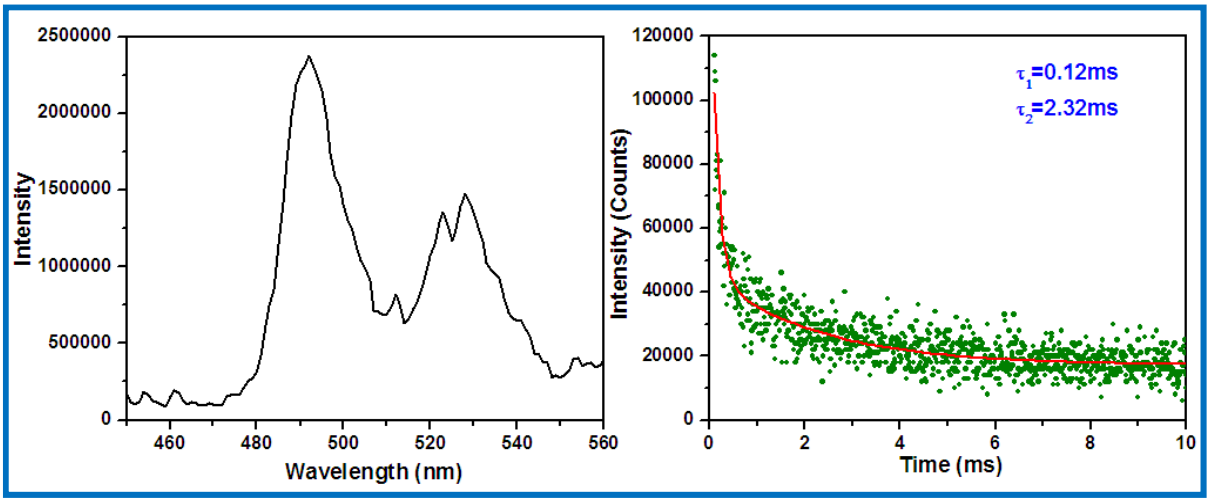

Fig. 3.6: (i) Phosphorescence spectra of **P**[1] hydrosol (sample-c), (ii) phosphorescence decay curve of **P**[1] hydrosol (sample-c) at room temperature; excitation: 336 nm and emission: 493 nm.

Thus in order to get some idea about the possible arrangement of **P**[1] in its aggregates, we have computed second orders Fukui parameter as local reactivity index for each atomic centre of **P**[1]. That a positive value of $f^{(2)}(r)$ at a particular atomic centre is a measure of its electrophilicity

and the negative value indicates its nucleophilicity. Our computed $f^{(2)}(r)$ for each atomic center of $\mathbf{P^1}$ is shown in ***Table 3.2***.

Table 3.2: Electrophilic $f+$ and nucleophilic f− condensed Fukui functions and second order Fukui parameter, $f^{(2)}(r)$ of Benz(a)anthracenemolecule calculated using DFT B3LYP 6-31G (d, p) level of theory.

Atom No.	$f^{+}\times 10^3$	$f^{-}\times 10^3$	$f^{(2)}(r)\times 10^3$		Atom No.	$f^{+}\times 10^3$	$f^{-}\times 10^3$	$f^{(2)}(r)\times 10^3$
1C	-16	-17	1		16H	-26	-22	-4
2C	-37	-38	1		17H	-27	-26	-1
3C	0	14	-14		18H	-29	-28	-1
4C	-3	5	-8		19H	-31	-25	-6
5C	-44	-51	7		20H	-32	-30	-2
6C	-63	-71	8		21H	-32	-31	-1
7C	-99	-111	12		22H	-29	-25	-4
8C	-105	-127	22		23C	-1	6	-7
9C	11	25	-14		24C	-51	-66	15
10C	7	12	-5		25C	-41	-29	-12
11C	-67	-59	-8		26C	-15	-26	11
12H	-28	-25	-3		27H	-12	-15	3
13C	-48	-56	8		28H	-27	-25	-2
14C	-40	-34	-6		29H	-27	-27	0
15C	-67	-73	6		30H	-24	-24	0

Our computed value of f $f^{(2)}(r)$ for the atomic centre 8C, 5C, 7C, 15C, 24C, 6C, 27H and 13C have positive $f^{(2)}(r)$ and atomic centre 9C, 4C, 3C, 14C, 25C, 18H, 23C and 20H have negative $f^{(2)}(r)$ value. The electrophilic centre of one molecule will show strong affinity towards the nucleophilic centre of its nearest neighbor. When two neighboring $\mathbf{P^1}$ molecule approach to each other, they will arrange in such a way that the atomic centre of one having +ve $f^{(2)}(r)$ value will face the atomic centers having –ve $f^{(2)}(r)$ value of the other. Atoms of each $\mathbf{P^1}$ unit involve in interaction with their $f^{(2)}(r)$ values are listed in ***Table 3.3***.

Table 3.3: Computed value of $f^{(2)}(r)$ of possible interacting atomic centers in Benz(a)anthracene dimer.

Benz(a)anthracene (upper)		Benz(a)anthracene (lower)	
Atom No.	$f^{(2)}(r) \times 10^3$	**Atom No.**	$f^{(2)}(r) \times 10^3$
8C	22	**9C**	-14
5C	7	**4C**	-8
3C	-14	**7C**	12
15C	6	**14C**	-6
25C	-12	**24C**	15
18H	-1	**6C**	8
23C	-7	**27H**	3
13C	8	**20H**	-2

Computed $f^{(2)}(r)$ values (***Table 3.3***) suggests that (8C-9C), (5C-4C), (3C-7C), (15C-14C), (25C-24C), (18H-6C), (23C-27H) and (13C-20H) atom pairs will interact strongly to give stable structure of $\mathbf{P^1}$ dimer. The possible arrangement of two neighboring $\mathbf{P^1}$ in its aggregated structure are shown in ***Scheme 3.2***.

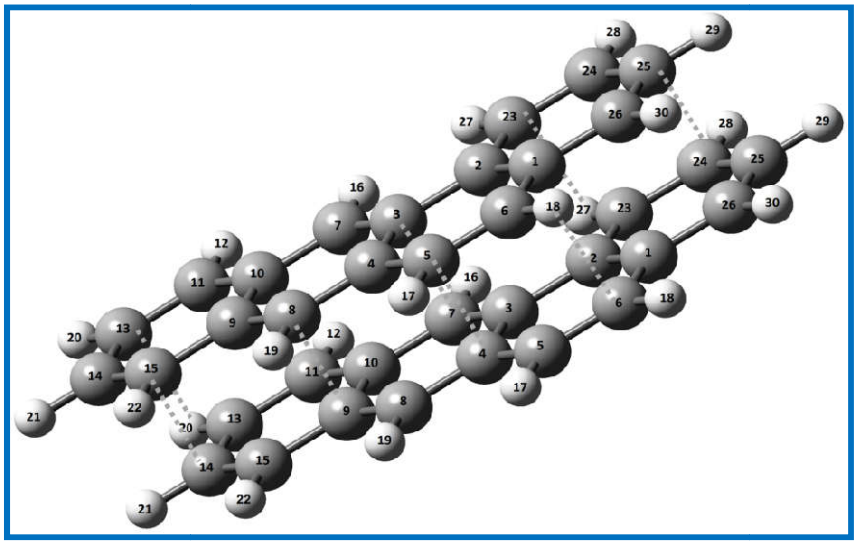

Scheme 3.2: Stacked conformer of $\mathbf{P^1}$ dimer.

3.4. Conclusions

Room temperature phosphorescence from any pure organic compound is rare in the literature. In this work, we discovered the useful phenomenon of crystal induced phosphorescence (CIP) in the aggregated structures of **P[1]**. **P[1]** shows intense structured fluorescence emission in its solution in good solvent, THF at room temperature. But no red shifted long lived emission components are observed at room temperature. On the other hand aggregated hydrosol of **P[1]** shows crystallization induced phosphorescence (CIP) emission at room temperature. In the crystalline state, the restricted intermolecular motions (RIM) help **P[1]** for appreciable excited triplet concentration upon photo excitation to its singlet excited state. The long lived red shifted emission arising from the low lying triplet state is further confirmed by cut off the short lived fluorescence with the help of a rotating chopper. The phosphorescence nature of emission is further supported by the long lifetime (ms) of the excited state of luminogen. Possible arrangement of two neighboring **P[1]** in the aggregated structure has been explained theoretically using the second order Fukui parameter as a local reactivity descriptor. "The molecular packing arrangement and intermolecular interactions, such as C–C and C–H, cooperatively locked the molecular conformation, thus restricting the rotational and large amplitude vibrational motion for each **P[1]** molecule. This phenomenon is known as the restricted intramolecular motion (RIM), permits to attaining a reasonable excited triplet population which allows the observation of room temperature phosphorescence emission.